The Combined NVSS–FIRST Galaxies (CoNFIG) sample – II. Comparison of space densities in the Fanaroff–Riley dichotomy

M. A. Gendre,[1]★ P. N. Best[2] and J. V. Wall[1]

[1]*Department of Physics and Astronomy, The University of British Colombia, 6224 Agricultural Road, Vancouver, BC V6T 1Z1, Canada*
[2]*Institute for Astronomy, Royal Observatory, Blackford Hill, Edinburgh EH9 3HJ*

ABSTRACT

This paper focuses on a comparison of the space densities of Fanaroff–Riley type I (FR I) and FR II sources at different epochs, with a particular focus on FR I sources.

First, we present the concluding steps in constructing the Combined NVSS–FIRST Galaxies (CoNFIG) catalogue, including new Very Large Array observations, optical identifications and redshift estimates. The final catalogue consists of 859 sources over four samples (CoNFIG-1, -2, -3 and -4 with flux density limits of $S_{1.4\,GHz} = 1.3, 0.8, 0.2$ and 0.05 Jy, respectively). It is 95.7 per cent complete in radio morphology classification and 74.3 per cent of the sources have redshift data.

Combining CoNFIG with complementary samples, the distribution and evolution of FR I and FR II sources are investigated. We find that FR I sources undergo mild evolution and that, at the same radio luminosity, FR I and FR II sources show similar space density enhancements in various redshift ranges, possibly implying a common evolution.

Key words: surveys – galaxies: active – galaxies: luminosity function, mass function – galaxies: statistics – radio continuum: galaxies.

1 INTRODUCTION

Radio active galactic nuclei (AGNs) are classified in various ways such as luminosity, spectral type or morphology. The Fanaroff–Riley (FR) classification (Fanaroff & Riley 1974) provides a classification of extended radio sources. The FR type I (FR I) objects have the highest surface brightness along the jets and core, reside in moderately rich cluster environments (Hill & Lilly 1991) and include sources with irregular structure (Parma et al. 1992). In contrast, FR II sources show the highest surface brightness at the lobe extremities, as well as more collimated jets, are found in more isolated environments and generally display stronger emission lines (Baum & Heckman 1989; Rawlings et al. 1989).

The FR I/FR II dichotomy is based purely on the appearance of the radio objects and, although some hypotheses exist (e.g. Bicknell 1995), the mechanisms differentiating the two populations are still unknown. If sources with different FR classes undergo different evolution, this might imply that their fundamental characteristics, such as the black hole spin or jet composition, are different too. However, the cut between FR I and FR II is somewhat ambiguous: hybrid sources showing jets FR I-like on one side and FR II-like on the other have been observed (Capetti et al. 1995).

In an initial modelling of the space density of radio AGN, Wall & Jackson (1997) and Jackson & Wall (1999) assumed that the cosmic evolution of radio loud AGN was based on a division of the radio sources into a high-luminosity component ($P_{178\,MHz} > 10^{25}$ W Hz^{-1} sr^{-1}) corresponding to FR IIs and a low-luminosity component showing no cosmic evolution, corresponding to FR Is. With the advent of large-scale redshift surveys for nearby galaxies, many authors, including Snellen & Best (2001), Willott et al. (2001), Sadler et al. (2002) and Rigby, Best & Snellen (2008), found significant evolution for low power sources – but mild evolution in comparison with that of the high-luminosity sources. Rigby et al. (2008) argued that if FR Is and FR IIs have similar evolution, the dual-population scheme could be reduced to a single-population model. Their sample was however confined to a small number of low flux density sources.

A dedicated study and comparison of FR I and FR II sources and their evolution, using large samples of sources of each type, is the key to understanding these populations and determining if the FR classification is valid or if a different classification, such as whether they display high- or low-excitation emission lines, is physically more relevant.

A further motivation for studying the cosmic behaviour of radio AGNs is to assess their contribution to feedback processes. The current paradigm for galaxy formation, hierarchical build-up in a cold dark matter (CDM) universe, implies that the most massive galaxies in the local Universe ought to be the largest and bluest and have the highest star-forming rate of all galaxies. Yet, observations show that they are red, old galaxies, and the bulk of star formation is observed at earlier epochs. This is known as downsizing, first described by Cowie et al. (1996).

★E-mail: mgendre@phas.ubc.ca

AGN negative feedback, in which the ignition of the nucleus in a star-forming galaxy ejects the gas into the intergalactic medium, is a possible way to understand this phenomenon. AGNs jets could indeed be responsible for reducing or even stopping star formation, breaking the hierarchical build-up (Silk & Rees 1998; Granato et al. 2001; Quilis, Bower & Balogh 2001). AGN can also have a positive feedback effect, whereby pressure from the jets compresses the interstellar medium (ISM) and induces star formation (Klamer et al. 2004; van Breugel et al. 2004). However, modelling of jet power and its relation to star formation have shown that the overall effect is a decrease in star-formation rate (Antonuccio-Delogu & Silk 2008).

If AGN feedback from the heating and ejection of gas in the ISM possibly suppresses star formation, it is reasonable to think that it should be related to the energy output from the jets. Best et al. (2006) studied the output energy from AGNs and concluded that heating dissipated in the host galaxy is dominated by low-luminosity radio sources, which tend to be confined predominantly to the size of the galaxy and its halo. Such sources also stay 'on' for a longer period of time than high-luminosity sources, allowing heat to be supplied pseudo-continuously. Schawinski et al. (2009) investigated the relation between the amount of molecular gas and AGN activity in galaxies and concluded that a low-luminosity AGN episode was sufficient to suppress residual star formation in early-type galaxies.

Establishing the potential space density behaviour of radio AGN is thus important in studying the precise role of the feedback mechanisms. Could feedback be linked to source morphology as it is to luminosity? Do FR I sources have a higher impact on star-formation rate than typically more powerful FR II sources?

The lack of a large comprehensive catalogue of morphologically classified radio sources has been a limiting factor in all these studies. This is the goal of the Combined NVSS–FIRST Galaxies (CoNFIG) catalogue, which we propose to use in modelling the radio luminosity function (RLF) of AGN.

This is the second paper in a series studying extended radio galaxies and their role in AGN feedback. Paper I (Gendre & Wall 2008) outlined the initial construction of the CoNFIG sample. This paper describes the complete catalogue, including optical identifications and redshift estimates, as well as a preliminary study of FR I and FR II space densities.

The structure of this paper is as follows. The construction of the catalogue is explained in Section 2 while Section 3 describes how the morphologies were determined. Optical identifications and redshift information are discussed in Section 4 and an overall summary of the catalogue is given in Section 5, along with the introduction of complementary data sets that will be used in the modelling. Section 6 describes the morphology-dependent luminosity distributions and the FR I/FR II source counts, as well as cosmic evolution of the RLF. Finally, Section 7 summarizes the results.

Throughout this paper, we assume a standard ΛCDM cosmology with $H_0 = 70 \, \mathrm{km \, s^{-1} \, Mpc^{-1}}$, $\Omega_M = 0.3$ and $\Omega_\Lambda = 0.7$.

2 THE CONFIG CATALOGUE

2.1 Catalogue definition

The CoNFIG catalogue consists of four samples, CoNFIG-1, -2, -3 and -4, which include all sources selected from the NRAO-VLA Sky Survey (NVSS) catalogue with $S_{1.4\,\mathrm{GHz}} \geq 1.3, 0.8, 0.2$ and $0.05 \, \mathrm{Jy}$ respectively in defined areas (see Fig. 1 and Table 1).

The NVSS (Condon et al. 1998) is a 1.4-GHz continuum survey covering the entire sky north of $\delta = -40°$ (corresponding to an area
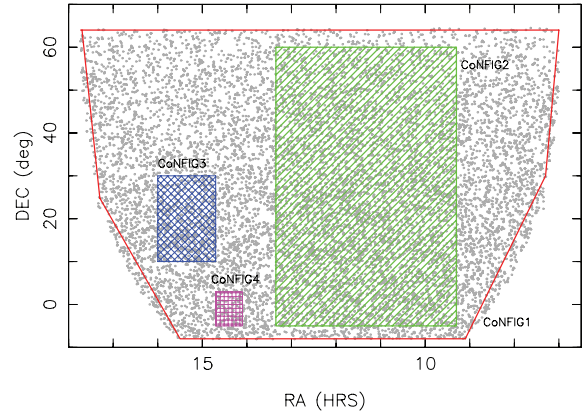
Figure 1. Map of the sample regions. Each sample is located in the north field of FIRST (grey area). CoNFIG-1 (solid contour), CoNFIG-2 (hatched), CoNFIG-3 (diagonally cross-hatched) and CoNFIG-4 (vertically cross-hatched) have flux density limits of 1.3, 0.8, 0.2 and 0.05 Jy, respectively. Definition of the regions and details of the samples can be found in Tables 1 and 2.

Table 1. Region corners for the CoNFIG samples ({RA; Dec.} in {h; °}) as shown in Fig. 1.

C-1	C-2	C-3	C-4
{17.7; 64.0}	{9.30; 60.0}	{14.7; 30.0}	{14.1; 3.0}
{7.0; 64.0}	{13.35; 60.0}	{16.0; 30.0}	{14.7; 3.0}
{7.3; 30.0}	{13.35; −5.0}	{16.0; 10.0}	{14.7; −3.5}
{17.3; 24.8}	{9.30; −5.0}	{14.7; 10.0}	{14.1; −3.5}
{15.5; −8.0}			
{9.1; −8.0}			

of 10.3 sr). The completeness limit is $\sim$2.5 mJy beam^{-1} with an rms of $\sim$0.45 mJy beam^{-1}. The catalogue from the survey contains over 1.8 million sources, implying a surface density of $\sim$50 sources per deg^2. It was carried out with the Very Large Array (VLA) in D and DnC configuration (the D configuration being the most compact VLA configuration with a maximum antenna separation of $\sim$1 km), providing an angular resolution of about 45-arcsec full width at half-maximum (FWHM).

Since the median angular size of faint extragalactic sources at the CoNFIG flux density levels is $\lesssim$10 arcsec (Condon et al. 1998), most sources in NVSS are unresolved, and the flux density measurements are quite accurate. However, the large beam size does not reveal precise structure of sources or determine positions accurate enough to establish unambiguous optical counterparts.

Very large sources resolved in NVSS within the initial samples, such as a few Third Cambridge Revised (3CRR) sources (Laing, Riley & Longair 1983), need to be considered. In some of these cases, two or more NVSS 'sources' with $S_{1.4\,\mathrm{GHz}} > S_{\mathrm{lim}}$ are actually components of a much larger resolved source. Multicomponent sources in which each component has $S_{1.4\,\mathrm{GHz}} < S_{\mathrm{lim}}$ but with a total flux density $S_{1.4\,\mathrm{GHz}} \geq S_{\mathrm{lim}}$, also need to be considered. For this purpose, NVSS sources with $S_{1.4\,\mathrm{GHz}} < S_{\mathrm{lim}}$ were selected and, if any other source in the catalogue was located within 4 arcmin of the listed source, the combination was set aside as a candidate extended source. The final decision on whether or not the sources were actually components of a resolved source was made by visual inspection of the NVSS contour plots.

A summary of each sample is given in Table 2. Because the area of the CoNFIG-2, -3 and -4 samples overlap with CoNFIG-1, all

Table 2. Characteristics of the CoNFIG samples, as described in Section 2.

	S_{lim} (Jy)	Area (deg^2)	Number of sources	Numbers not in C-1
C-1	1.30	4924	273	-
C-2	0.80	2915	243	132 (54.3 per cent)
C-3	0.20	370	286	270 (94.4 per cent)
C-4	0.05	52	185	184 (99.4 per cent)

statistics estimated from CoNFIG-2, -3 and -4 use only sources with $S_{lim} < S_{1.4\,GHz} < 1.3$ Jy.

2.2 Spectral indices

In order to compute the radio luminosity, the spectral index α (defined as $S_\nu \propto \nu^\alpha$) of each source needs to be determined. To achieve this, flux densities at different frequencies for each source were compiled and the spectral index computed following the relation:

$$\alpha = \frac{\Delta \log(S)}{\Delta \log(\nu)}. \tag{1}$$

A summary of the different frequencies and corresponding surveys used to retrieve the flux density information can be found in Gendre & Wall (2008). We were able to compute the low-frequency spectral index (with 178 MHz $\leq \nu \leq$ 1.4 GHz) for 99.6, 97.7, 89.3 and 52.7 per cent of the sources in CoNFIG-1, -2, -3 and -4, respectively.

3 MORPHOLOGY
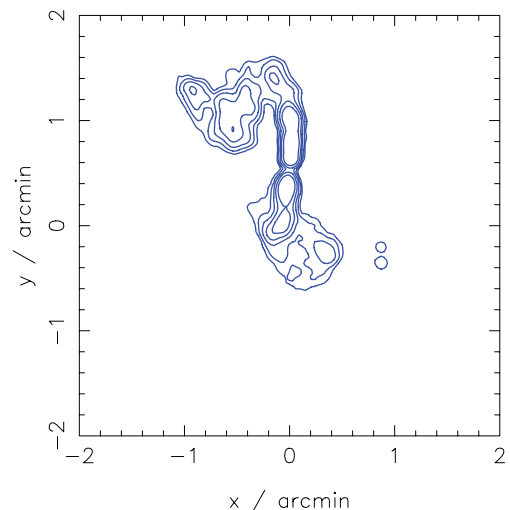
3.1 Initial classification

The initial morphologies were determined either from previously referenced work or following the procedure described by Gendre & Wall (2008), primarily by looking at Faint Images of the Radio Sky at Twenty-cm survey (FIRST) and NVSS contour plots.

The FIRST (White et al. 1997) is another 1.4-GHz continuum survey with the VLA, covering an area of ~9030 deg^2 including the North Galactic Pole. The completeness limit is ~1 mJy beam^{-1} with a typical rms of 0.15 mJy beam^{-1}. The survey yielded ~811 000 sources, implying a surface density of ~90 sources per deg^2. It was carried out in B configuration (the B configuration having a maximum antenna separation of ~10 km), which provides an angular resolution of about 5-arcsec FWHM. This survey complements the NVSS survey well, providing a beam size small enough to resolve the structure of most nearby extended radio sources and source positions to better than 1 arcsec to enable cross-waveband identification.

If the FIRST/NVSS contour plot displays distinct hotspots at the edge of the lobes (as in Fig. 2), and the lobes are aligned, the source was classified as FR II. Sources with collimated jets showing hotspots near the core and jets were classified as FR I (see Fig. 3). Wide-angle tail (Leahy 1993) sources as well as most irregular looking sources (Parma et al. 1992) were also classified as FR I. Sources of size smaller than 1 arcsec or previously classified as quasi-stellar objects (QSOs) were classified as 'compact' while extended sources for which the FR I/FR II classification was impossible to determine were classified as 'uncertain'.

3.2 VLA observations

In addition to the observations described by Gendre & Wall (2008), radio observations of 213 extended CoNFIG sources with previ-
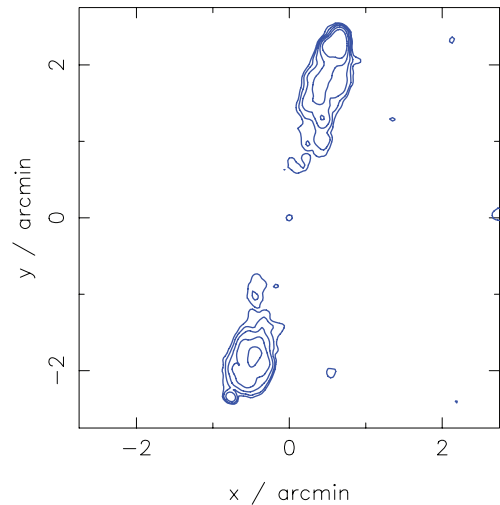
Figure 2. FIRST contour plot of a characteristic example of an FR II source, 3C 223. The hotspots are located at the ends of the aligned lobes.

Figure 3. FIRST contour plot of a characteristic example of an FR I source, 3C 272.1 (M84). The regions of highest surface brightness are located along the jets.

ously uncertain morphological classification were made at 1.4 GHz using the VLA in A configuration. These observations included polarization measurements for 31 sources as preliminary work for a possible study of the morphology-dependent polarized source count.

The A configuration, the most extended VLA configuration with a maximum antenna separation of ~36 km, provides a synthesized beam of 1.4-arcsec FWHM at 1.4 GHz. Three frequency bands were used: (1) two IFs of 1464.9 and 1385.1 MHz, with a bandwidth of 50 MHz (2) two IFs of 1372.5 and 1422.5 MHz, with a bandwidth of 25 MHz and (3) two IFs of 1425.5 and 1397.5 MHz, with a bandwidth of 25 MHz. Frequency bands 2 and 3 were used in the polarization measurements.

The exposure time was computed for each source such as to provide a signal-to-noise ratio of at least 5, and the exposures were split into two or three separate integrations to improve *uv* coverage. The primary calibrator 3C 286 (1331+305) was observed several

times during the run. Nearby secondary calibrators were observed approximately every 30 min to provide phase calibration. All data were reduced using standard procedures incorporated within the AIPS software provided by the National Radio Astronomy Observatory (NRAO).

3.3 Final classification

62.5 per cent of sources in the CoNFIG sample were classified either as FR I (I) or FR II (II). Following the unified model of AGN (Jackson & Wall 1999) core-jet sources were classified as FR II. Hybrid sources, showing jets FR I-like on one side and FR II-like on the other (Capetti et al. 1995), were classified according to the characteristics of the most prominent jet. Extended sources for which FR I/FR II identification was ambiguous were classified as uncertain (U). Sources with size smaller than 3 arcsec were classified as compact (C) or (C*), depending on whether or not the source was confirmed compact from the Very Long Baseline Array calibrator list (see Beasley et al. 2002; Fomalont et al. 2003; Petrov et al. 2006; Kovalev et al. 2007) or the Pearson–Readhead survey (Pearson & Readhead 1988). Finally, sources of type (S*) correspond to confirmed compact sources which show a steep ($\alpha \leq -0.6$) spectral index. These are probably compact steep-spectrum sources.

The final classification for each source is shown in Appendix A (online only – see Supporting Information) and the distribution of morphological types is presented in Table 3. Contour plots of extended sources, including the VLA observation presented in Section 3.2, are presented in Appendix B (online only – see Supporting Information). In order to study the evolution of the space density of FR I and FR II sources accurately, each extended source was assigned a sub-classification – confirmed (c) or possible (p) – depending on how clearly the source showed either FR I or FR II characteristics.

The complete catalogue consists of 859 sources, with 71 (8.3 per cent) FR Is (50 confirmed, 21 possible), 466 (54.2 per cent) FR IIs (390 confirmed, 76 possible), 285 (33.2 per cent) compact sources and 37 (4.3 per cent) uncertain sources.

Table 3. Morphology of the sources in the CoNFIG samples. The morphology of each source was determined by looking at FIRST and NVSS contour plots or from VLA observations as described in Sections 3.1 and 3.2. Sources of size smaller than 3 arcsec or previously classified as QSOs were classified as 'compact' (C) while extended sources for which the FR I/FR II classification was impossible to determine were classified as 'uncertain' (U). In each case, the corresponding percentage of sample is given in *italic*.

	C-1	C-2	C-3	C-4	Tot.
	Per cent of sample				
FR I	25	7	22	17	71
	9.2	*5.3*	*8.1*	*9.2*	*8.3*
FR II	149	75	152	90	466
	54.6	*56.8*	*56.3*	*48.9*	*54.2*
C	86	47	88	64	285
	31.5	*35.6*	*32.6*	*34.8*	*33.2*
U	13	3	8	13	37
	4.8	*2.3*	*3.0*	*7.1*	*4.3*

Table 4. Numbers of SDSS and 2MASS optical identifications for the CoNFIG samples. In each cases, the corresponding percentage of sample is given in *italic*.

			SDSS			2MASS
	All	FR I	FR II	C	U	All
			Per cent of sample			
C-1	233	25	125	73	10	117
	85.3	*100*	*83.9*	*84.9*	*76.9*	*42.9*
C-2	108	6	62	37	3	44
	81.8	*85.7*	*82.7*	*78.7*	*100*	*33.3*
C-3	190	20	111	53	6	47
	70.4	*90.9*	*73.0*	*60.2*	*75.0*	*17.4*
C-4	110	17	52	37	4	22
	59.8	*100*	*57.8*	*57.8*	*30.8*	*12.0*
Tot.	641	68	350	200	23	230
	74.6	*95.8*	*75.1*	*70.2*	*62.2*	*26.8*

4 OPTICAL IDENTIFICATIONS AND REDSHIFTS

A preliminary search for counterparts was performed using the unified catalogue of radio objects of Kimball & Ivezić (2008),[1] and optical identifications were obtained, principally from the Sloan Digital Sky Survey (SDSS; York et al. 2000).

The SDSS, with the 2.5-m telescope at Apache Point Observatory, New Mexico, has imaged one-quarter of the entire sky in *ugriz* magnitudes,[2] as well as performing a spectroscopic redshift survey. The seventh data release (DR7; Abazajian et al. 2009) imaging survey contains a total of 357 million objects over 11 663 deg² while the spectroscopic survey contains 1.6 million objects over 9380 deg².

K_S-band photometric information was obtained from the Two Micron All Sky Survey (2MASS; Skrutskie et al. 2006) . The 2MASS is a near-infrared survey using 1.3-m telescopes at Mount Hopkins in Arizona and CTIO in Chile. It aimed at imaging the entire sky in *J*, *H* and K_S magnitudes. The now-complete catalogue, divided into a point source and an extended source (semimajor axis >10 arcsec in size) catalogue, contains 472 million sources over 99.998 per cent of the sky.

A summary of the number of identified optical counterparts is given in Table 4.

4.1 Spectroscopic and photometric redshifts

Spectroscopic redshifts were obtained for 45.5 per cent of the catalogue (see Table 5) using either the SIMBAD[3] data base or the SDSS DR7 catalogue.

Because redshift information is essential to computing space densities and examining their evolution, we estimated redshifts for sources with no spectroscopic data available.

For a number of sources with an SDSS counterpart identified but with no spectroscopic information available, photometric redshifts were retrieved from the SDSS *photoz2* catalogue (Oyaizu et al.

---

[1] http://www.astro.washington.edu/akimball/radiocat/
[2] The limiting magnitudes at the detection limit given in Abazajian et al. (2009) correspond to a 95 per cent detection repeatability for point sources. However, for galaxies, these are typically between half a magnitude and a magnitude brighter at the same signal-to-noise ratio (from SDSS project book: http://www.astro.princeton.edu/PBOOK/camera/camera.htm).
[3] http://simbad.u-strasbg.fr/simbad

Table 5. Distribution and ranges of redshifts for the CoNFIG samples. Spectroscopic redshifts are retrieved either from the SIMBAD data base or from the SDSS catalogue. Photometric redshifts are either obtained from the SDSS *photoz2* catalogue or estimated using either the SDSS mag–z relation defined by equations (2–4) or the K_S–z relation defined by equations (5) and (6). In each case, the corresponding percentage of sample is given in italic.

		C-1	C-2	C-3	C-4
Total number of sources in sample					
		273	132	270	184
Redshift types					
Per cent of sample					
Spectro.		226	67	54	44
		82.8	*58.8*	*20.0*	*23.9*
Photo.	*photoz2*	29	33	71	35
		10.6	*25.0*	*26.3*	*19.0*
	SDSS mag–z	5	13	38	17
		1.8	*5.3*	*13.3*	*9.2*
	K_S–z	3	1	2	0
		1.1	*0.8*	*0.7*	*0.0*
Total		263	114	165	96
		96.3	*86.4*	*61.1*	*52.2*
	FR I	25	7	21	17
		100	*100*	*95.4*	*100*
	FR II	145	65	112	52
		97.3	*86.7*	*73.7*	*57.8*
	C	80	39	26	23
		93.0	*83.0*	*29.5*	*35.9*
	U	13	3	6	4
		100	*100*	*75.0*	*30.8*
Redshift ranges					
	min.	0.003	0.011	0.018	0.006
All	max.	3.530	2.707	2.408	2.677
	mean	0.711	0.760	0.623	0.828
	med.	0.555	0.599	0.564	0.695
	min.	0.003	0.011	0.032	0.006
FR I	max.	0.269	0.309	1.847	1.531
	mean	0.071	0.128	0.264	0.261
	med.	0.049	0.099	0.116	0.150
	min.	0.036	0.098	0.062	0.138
FR II	max.	2.183	1.711	2.408	2.677
	mean	0.637	0.660	0.674	0.938
	med.	0.523	0.566	0.604	0.800
	min.	0.034	0.160	0.018	0.133
C	max.	3.530	2.707	1.764	2.235
	mean	1.024	1.050	0.665	1.026
	med.	0.880	0.795	0.580	0.725

2008), which covers SDSS galaxies with $r \leq 22.0$. For other galaxies (excluding the 285 sources identified as 'compact', which are most likely QSOs), redshifts were estimated using a magnitude–redshift relationship computed from SDSS-identified CoNFIG non-compact (i.e. non-QSO) sources with spectroscopic redshifts:

$$\log(z) = -3.599 + 0.170i \qquad (2)$$

$$\log(z) = -3.609 + 0.175z \qquad (3)$$

$$\log(z) = -3.660 + 0.169r. \qquad (4)$$

The relations are shown in Fig. 4 and were used to estimate photometric redshifts for 73 sources.

K_S–z relations were also obtained using data from CoNFIG non-compact sources having both spectroscopic redshifts and K_S-band information from the 2MASS extended and point source catalogues:

$$\log(z) = -3.515 + 0.204K_S \qquad \text{2MASS extended sources,} \qquad (5)$$

$$\log(z) = -4.800 + 0.279K_S \qquad \text{2MASS point sources.} \qquad (6)$$

The relations, shown in Fig. 5, provide good estimates of redshifts up to $K_S = 15.5$. They were used to estimate photometric redshifts for six sources which had no SDSS spectroscopic or photometric redshifts available but had 2MASS counterparts ($K_S \leq 15.5$).

Overall, 74.3 per cent of the sources in the CoNFIG catalogue have spectroscopic or photometric redshift information available, with mean and median redshifts of $z_{mean} = 0.714$ and $z_{med} = 0.588$. The redshift distributions, by samples and morphological types, are shown in Fig. 6.

### 4.2 Sources with no redshift information

A total of 221 sources in the CoNFIG catalogue, mostly in CoNFIG-3 and -4, have no redshift information available. 104 of these sources are of morphological type I, II or U (we will ignore sources of type C for the time being, being only interested in the study of extended radio sources). One way to include these sources in the space density modelling is to assign an estimated redshift to each of them (by the procedures described below), compute the RLF, repeat the procedure and average the results.

Based on SDSS non-detection, we can determine a lower redshift limit for these sources. The i band being effectively the deepest SDSS band for objects with the typical colours of high-redshift radio galaxies, equation (2) was used to determine the lower limit, yielding a value of $z_{lim} \simeq 1.0$. To account for the spread in the i–z relation, the estimate of the limit was drawn randomly from a Gaussian of variance 0.1, centred on $z_{lim} = 1.0$.

Our next step was to use the (admittedly naive) assumption that the redshift of the radio source could be estimated from the distribution of measured or estimated redshifts for sources of similar flux density. For each of the 113 sources, we derived the sample of sources with redshift information available and flux densities within the range of a tenth to ten times the flux density of the source with no redshift. The redshift distribution of this sample was computed and fitted with a polynomial; the region of this polynomial above the calculated redshift limit was then normalized to determine the redshift probability distribution for the source.

To complete the catalogue redshift distributions, we determined that each source with no redshift will contribute a fraction to each redshift bin, following its assigned probability distribution. For space densities computation (see Section 6), approximated redshifts were assigned to each source by making random realizations following the probability distribution, repeating the process in a Monte Carlo manner.

Because most of the approximate redshifts are greater than $z = 0.3$, the redshift upper limit used to define the local universe, the results of the local RLF (LRLF) are completely unaffected by redshift uncertainties. As the redshift lower limits used in the computation of the approximate redshifts are mostly $z \geq 1.0$, results out to $z \sim 1.0$ are also not significantly affected. Over the range $1.0 \leq z \leq 2.0$, the results are likely to be impacted. Nevertheless, the fact that the redshift distribution is well determined over that range implies that the impact is perhaps not severe. Beyond $z = 2.0$, results would be unreliable as the redshift distribution is not well
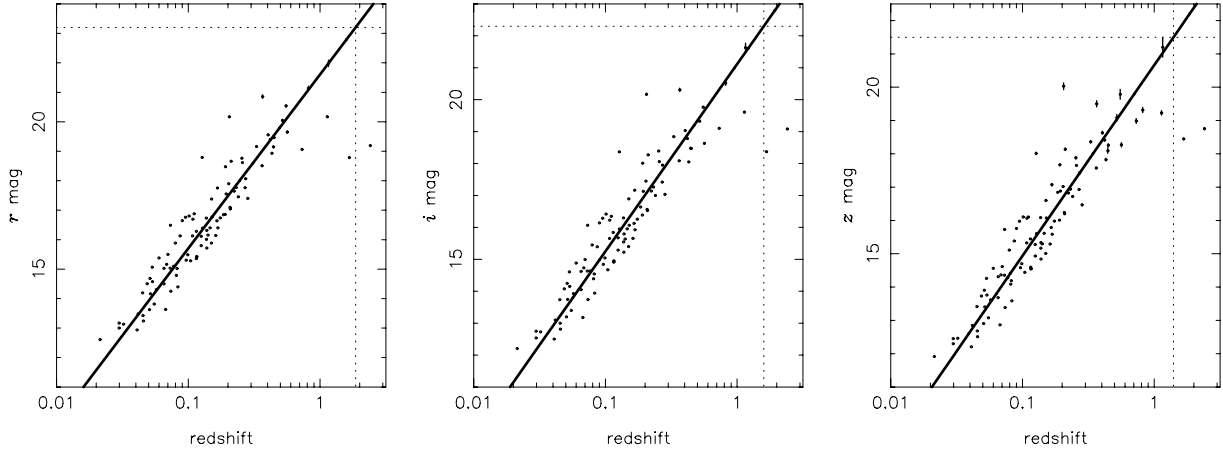
Figure 4. The SDSS magnitude–redshift relations were computed by finding the best fit (solid lines) to data from CoNFIG non-QSO sources having both spectroscopic redshift and SDSS magnitude information (dots). The relations (equations 2–4) were used to estimate photometric redshifts for sources not in the *photoz2* catalogue, but with an SDSS counterpart.
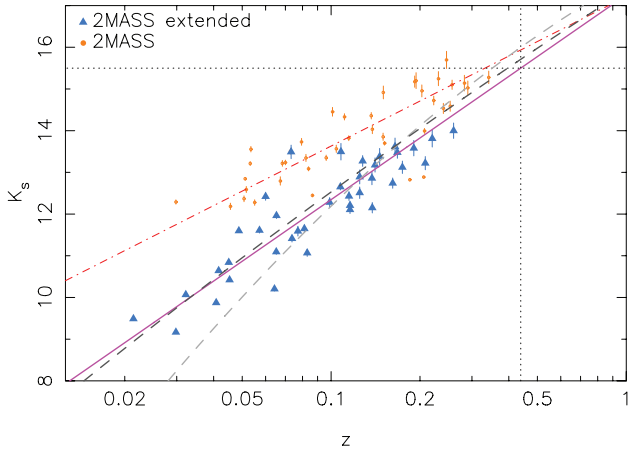
Figure 5. The K_S–z relation was computed by finding the best fit (solid pink and dot–dashed red lines, respectively) to data from CoNFIG non-QSO sources having both spectroscopic redshift and K_S-band information from the 2MASS extended (blue triangles) and point source (orange dots) catalogues. The relations (equations 5–6) were used to estimate photometric redshifts for sources with a magnitude $K_S \leq 15.5$, which corresponds to an upper estimated redshift limit of $z = 0.43$ (dotted lines) from the extended source relation. For comparison, the K–z relations from CENSORS (Brookes et al. 2006) and (Willott et al. 2003) are shown in light and dark grey dashed lines, respectively.

determined and the use of approximate redshifts may have introduced significant biases.

5 CATALOGUE SUMMARY AND COMPLEMENTARY SAMPLES

The CoNFIG catalogue (Table 6, Appendix A1) consists of 859 sources over four samples, CoNFIG-1, -2, -3 and -4 with flux density limits $S_{1.4\,GHz} = 1.3, 0.8, 0.2$ and 0.05 Jy, respectively. Spectral indices were computed for 86.0 per cent of the sources using flux densities at different frequencies for each source. The catalogue is 95.7 per cent complete for radio morphologies and 74.3 per cent complete for redshift information.

Sources were morphologically classified into six categories, using NVSS, FIRST and VLA 1.4-GHz A-configuration observation contour plots as well as previously referenced information. Sources

of type I and II correspond to Fanaroff & Riley (1974) morphologies; extended sources for which FR I/FR II identification was uncertain were classified as type U; sources with size smaller than 1 arcsec were classified as C type or C* type, depending on whether or not the source was confirmed compact; sources of S* type correspond to confirmed compact sources which show a steep spectral index.

Optical counterparts were obtained from the SDSS and 2MASS catalogues for 74.6 and 26.8 per cent of the sources, respectively. Spectroscopic redshift information was retrieved from SDSS and the SIMBAD data base, while photometric redshifts (or redshift estimates) were compiled from the SDSS *photoz2* catalogue, or using the K_S–z or SDSS mag–z relations (equations 2–6).

To improve the flux density coverage of the catalogue, three complementary samples were appended (Appendices A2, A3 and A4).

(i) The 3CRR catalogue (Laing et al. 1983) is complete to $S_{178\,MHz} = 10$ Jy and contains 173 sources over an area of 4.2 sr. The conversion from $S_{178\,MHz}$ to $S_{1.4\,GHz}$ with $\alpha = 0.8$ yield a flux density limit of $S_{1.4\,GHz} \approx 1.92$ Jy. In order to maximize the completeness of the sample at 1.4 GHz, we increased the flux density limit to $S_{1.4\,GHz} = 3.5$ Jy. The compiled spectral indices were used in the conversion for each 3CRR source. After excluding sources already present in the CoNFIG samples, 38 sources were selected to complement the CoNFIG catalogue. All sources were morphologically classified, either using the classification of Laing et al. (1983) or following the method described in Section 3, and the sample includes eight FR I, 24 FR II and six compact sources.

(ii) The Combined EIS–NVSS Survey Of Radio Sources (CENSORS) sample (Best et al. 2003) is complete to $S_{1.4\,GHz} = 7.2$ mJy and contains 136 sources selected from NVSS over the 6 deg^2 of the ESO Imaging Survey (EIS) Patch D. The sample has spectroscopic redshifts for 68 per cent of the sources, and optical or near-IR identifications (giving redshift estimates) for almost all of the remainder.

Little radio morphological classification of the CENSORS sources has been done as the image resolution is often not high enough to identify the source morphology. For this reason, the VLA observation program described in Section 3.2 also included 40 CENSORS sources, allowing us to morphologically classify 84.5 per cent of the CENSORS sources. The sample includes 13 FR I, 64 FR II, 38 compact and 21 uncertain sources.
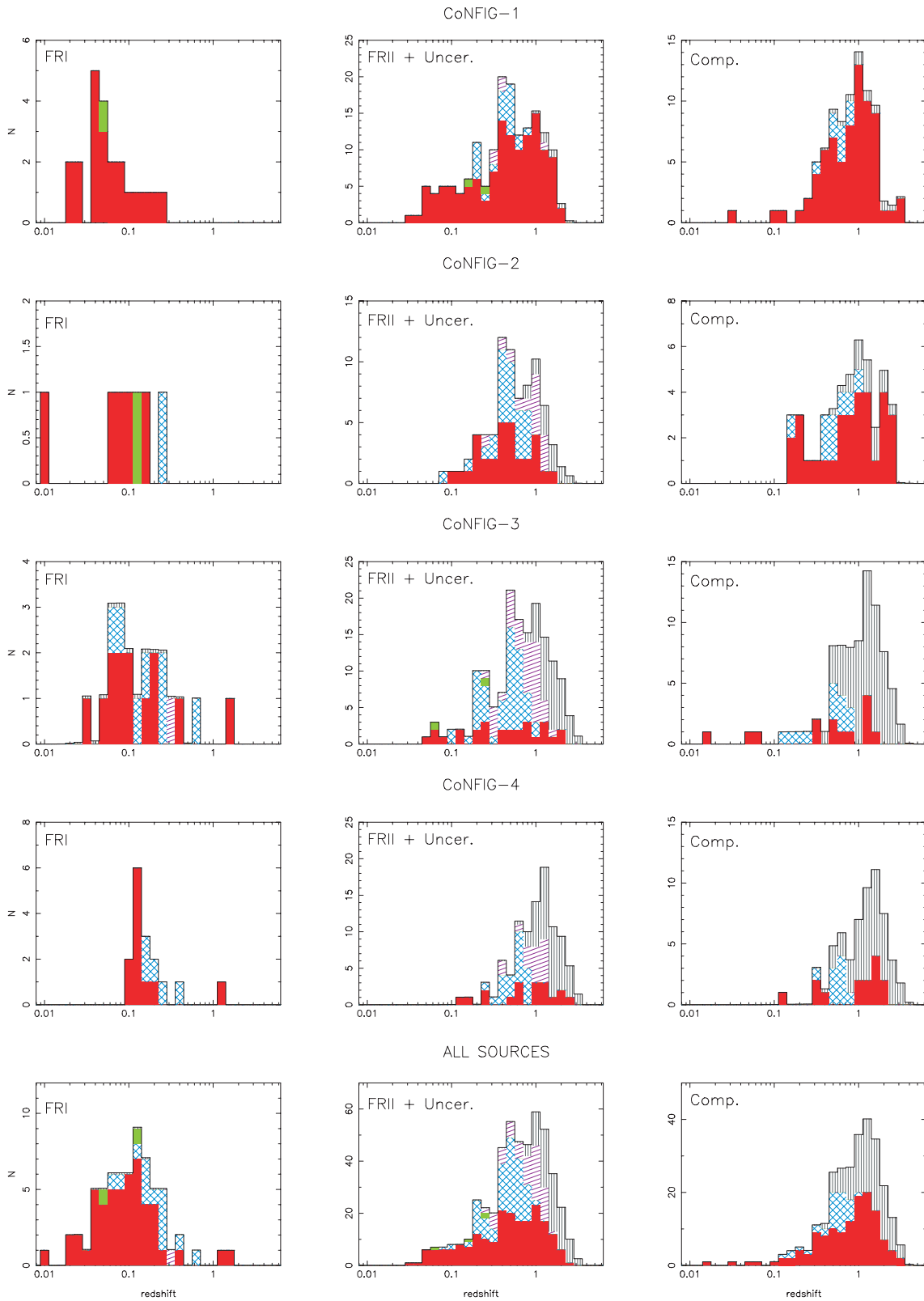
Figure 6. Redshift distribution of the sources in the CoNFIG catalogue for each morphological type. Sources with spectroscopic, photometric *photoz2*, K_S–z estimated and SDSS mag–z estimated redshifts are represented by the red solid, blue cross-hatched, green solid and purple diagonally hatched columns. The estimated contribution from sources with no redshift information available (Section 4.2) is shown in black vertically hatched columns.

Table 6. CoNFIG-1 Data Table (example).

	(1)	(2)	(3)	(4)	(5)	(6)	(7)	(8)	(9)	(10)	(11)	(12)	(13)	(14)	(15)	(16)
1	07 13 38.15	+43 49 17.20	B0710+439	2011.4	0.82	C*	0.5180	0.0010	S	07 13 38.10 +43 49 17.00[o]						
2	07 14 24.80	+35 34 39.90	B0711+35	1467.1	0.41	C*	1.6260	0.0001	S	07 14 24.82 +35 34 39.80[o]						
3	07 16 41.09	+53 23 10.30	4C 53.16	1501.4	−0.63	II[p]	0.0643	0.0939	S	07 16 41.21 +53 23 09.60	21.9	21.1	20.5	19.6	19.7	10.2[e]
4	07 35 55.54	+33 07 09.60	4C 33.21	2473.1	−0.56	C	0.7010	0.0014	P	07 35 55.57 +33 07 09.59	17.0	16.5	16.6	16.6	16.7	14.0
5	07 41 10.70	+31 12 00.40	J0741+3111	2284.3	0.38	C*	0.6300	0.0004	S	07 41 10.71 +31 12 00.22	15.7	15.5	15.6	15.4	15.3	12.9
6	07 45 42.13	+31 42 52.60	4C 31.30	1357.8	−0.55	II[c]	0.4608	0.0004	S	07 45 41.67 +31 42 56.70						
7	07 49 48.10	+55 54 21.00	DA 240	1660.4	−0.44	II[c]	0.0360	0.0001	S	07 48 34.70 +55 48 59.00[o]						
8	07 58 28.60	+37 47 13.80	NGC 2484	2717.9	−0.68	I[c]	0.0408	0.0002	S	07 58 28.11 +37 47 11.87	15.7	13.8	12.9	12.5	12.2	9.9[e]
9	07 59 47.26	+37 38 50.20	4C 37.21	1691.2	−0.84	II[c]										
10	08 01 35.32	+50 09 43.00	TXS 0757+503	1471.7	−1.02	II[p]	0.4855	0.0419	P	08 01 35.35 +50 09 43.99	22.2	21.6	20.6	20.0	19.3	12.4[e]
11	08 05 31.31	+24 10 21.30	3C 192	5330.6	−0.67	II[c]	0.0600		S	08 05 35.00 +24 09 50.36	18.1	16.2	15.4	14.9	14.6	
12	08 10 03.67	+42 28 04.00	3C 194	2056.6	−0.78	II[c]	1.1840		S	08 10 03.60 +42 28 04.00[o]	22.0					
13	08 12 59.48	+32 43 05.60	4C 32.24	1522.5	−0.68	II[c]	0.4306	0.0047	I	08 13 00.27 +32 42 43.71	18.6	20.7	19.8	19.0	18.4	14.8
14	08 13 36.07	+48 13 01.90	3C 196	15010.0	−0.75	II[c]	0.8710		S	08 13 36.07 +48 13 02.64	20.7	17.9	17.7	17.5	17.3	
15	08 19 47.55	+52 32 29.50	4C 52.18	2104.2	−0.62	II[c]	0.1890		S	08 19 47.51 +52 32 27.13	19.1	19.0	17.9	17.4	17.0	
16	08 21 33.77	+47 02 35.70	3C 197.1	1787.1	−0.75	II[c]	0.1280	0.0012	S	08 21 33.61 +47 02 37.36	21.0	17.7	16.8	16.3	16.0	13.5[e]
17	08 21 44.02	+17 48 20.50	4C 17.44	1875.1	−0.57	C[c]	0.2960	0.0002	S	08 21 44.02 +17 48 20.30	20.3	19.6	18.1	17.6	17.2	14.9
18	08 23 24.72	+22 23 03.70	4C 22.21	2272.4	−0.34	C*	2.2103	0.0013	S	08 23 24.76 +22 23 03.30	18.2	19.8	19.3	18.9	18.5	15.4
19	08 24 47.27	+55 52 42.60	4C 56.16A	1449.4	−0.25	C*	1.4181	0.0016	S	08 24 47.24 +55 52 42.71	18.3	18.1	17.9	17.8	17.8	
20	08 24 55.43	+39 16 41.80	4C 39.23	1480.8	−0.56	C*	1.2160	0.0010	S	08 24 55.48 +39 16 41.92	21.7	18.1	18.1	17.6	17.3	14.2
21	08 27 25.40	+29 18 44.80	3C 200	2043.1	−0.92	II[c]	0.4580		S	08 27 25.38 +29 18 45.04	19.2	20.4	19.1	18.5	18.0	15.3
22	08 31 10.00	+37 42 09.90	4C 37.24	2259.6	−0.65	C	0.9188	0.0014	S	08 31 10.01 +37 42 09.58	26.9	18.7	18.6	18.6	18.4	
23	08 33 18.80	+51 03 07.80	4C 51.25	1313.5	−0.81	II[c]	0.5621	0.0419	P	08 33 18.72 +51 03 06.88	23.0	22.3	20.5	19.6	19.2	
24	08 34 48.37	+17 00 46.10	3C 202	1882.8	−0.72	C[c]	0.6237	0.1740	P	08 34 48.22 +17 00 42.44	19.6	22.4	21.7	21.1	21.9	
25	08 34 54.91	+55 34 21.00	4C 55.16	8283.1	−0.01	II	0.2412	0.0014	S	08 34 54.90 +55 34 21.11	20.3	17.9	16.7	16.1	15.8	
26	08 37 53.51	+44 50 54.60	4C 45.17	1528.9	−0.60	II[c]	0.2072	0.0009	S	08 37 52.76 +44 50 25.95	17.9	18.4	17.1	16.6	16.2	14.0
27	08 39 06.50	+57 54 13.40	3C 205	2257.7	−0.86	II	1.5360		S	08 39 06.54 +57 54 17.06	18.7	17.4	17.0	16.6	16.5	14.5
28	08 40 47.70	+13 12 23.90	3C 207	2613.0	−0.81	II[c]	0.6804	0.0010	S	08 40 47.59 +13 12 23.62	25.6	18.1	18.0	17.9	17.7	15.0
29	08 43 31.63	+42 15 29.70	B3 0840+424A	1409.7	−0.41	C*[c]	0.8393	0.1758	P	08 43 31.64 +42 15 29.38	16.3	22.6	21.3	21.3	20.2	
30	08 47 53.83	+53 52 36.80	NGC 2656	1542.3	−0.58	I	0.0453	0.0002	S	08 47 53.07 +53 52 34.25	16.5	14.3	13.4	13.0	12.7	10.4[e]
31	08 47 57.00	+31 48 40.50	4C 31.32	1482.0	−0.52	II[p]	0.0673	0.0003	S	08 47 59.05 +31 47 08.34	17.9	14.5	13.6	13.2	12.9	12.8
32	08 53 08.83	+13 52 55.30	3C 208	2364.3	−0.97	II[c]	1.1115	0.0014	S	08 53 08.61 +13 52 54.84	19.8	17.9	17.6	17.6	17.8	
33	08 54 39.35	+14 05 52.10	3C 208.1	2163.8	−0.71	II[c]	1.0200		S	08 54 39.32 +14 05 51.86	16.4	19.6	19.3	19.3	19.2	
34	08 54 48.87	+20 06 30.70	PKS 0851+202	1511.8	0.21	C*[p]	0.4190	0.0016	P	08 54 48.87 +20 06 30.71	22.8	15.8	15.4	15.0	14.7	11.8[e]
35	08 57 40.64	+34 04 06.40	3C 211	1798.4	−0.77	II[c]	0.4789	0.0618	S	08 57 40.28 +34 04 04.91	23.3	21.9	20.6	19.8	19.4	
36	08 58 10.07	+27 50 50.80	3C 210	1807.8	−0.83	II[c]	1.1690		S	08 58 10.04 +27 50 54.17	21.0	22.6	21.5	21.0	20.2	
37	08 58 41.51	+14 09 43.80	3C 212	2370.8	−0.87	II[c]	1.0430		S	08 58 41.45 +14 09 44.78	21.0	20.0	19.1	18.8	18.6	15.3
38	09 01 05.40	+29 01 45.70	3C 213.1	2003.4	−0.58	II[p]	0.1940	0.0002	S	09 01 05.26 +29 01 46.92	20.1	18.5	17.6	17.1	16.9	15.2
39	09 03 04.04	+46 51 04.70	4C 47.29	1754.9	−0.39	C*	1.4710	0.0024	S	09 03 04.01 +46 51 04.21	19.3	19.3	18.9	18.7	18.7	
40	09 06 31.88	+16 46 13.00	3C 215	1586.2	−0.95	II[c]	0.4115	0.0003	S	09 06 31.80 +16 46 12.00	25.1	22.3	22.6	20.8	21.0	15.5

(iii) The Lynx and Hercules sample (Rigby, Snellen & Best 2007) is complete to a catalogue flux limit of $S_{1.4\,GHz} = 0.5\,$mJy, from radio images with initial flux density limits of 0.07–0.09 mJy beam^{-1}. It contains 81 sources within an area of 0.6 deg^2. It is complete in redshift estimation (49 per cent spectroscopic and 51 per cent photometric) and 95.6 per cent of the sample members have morphological classification, including 57 FR I, 18 FR II and six uncertain sources.

The final list, including the complementary samples, contains 1114 sources and is 75.9 per cent complete for redshift information and 94.2 per cent complete for radio morphologies. It includes a total of 136 FR I (78 confirmed, 58 possible) and 571 FR II (477 confirmed, 94 possible) sources, making it one of the largest, most comprehensive data bases of morphologically classified radio sources and an important tool in the study of AGN space densities.

6 SOURCE STATISTICS AND EVOLUTION

The main goal of the CoNFIG catalogue is to produce a comprehensive catalogue of morphologically classified radio sources to be used in the modelling of the RLF of AGN, in order to investigate their evolution and the role of the different types in feedback processes. For this purpose, we computed the luminosity distributions and source counts based on morphological classification, to be used in the RLF modelling.

6.1 Luminosity distribution and the *P–z* plane

The luminosity distribution is computed for each morphological type (FR I, FR II, C and U) for sources with available redshift infor-

mation, using the 1.4-GHz flux density and spectral index values of each source. When the latter was unavailable, a value of $\alpha = -0.8$ was used. This introduced a minimal bias in the results, since extended sources in the CoNFIG samples have a median spectral index of -0.75 and less than 6 per cent of them have $\alpha \geq -0.5$. Finally, sources with no redshift information were included, with redshifts as estimated in Section 4.2, and the resulting distributions are shown in Fig. 7.

A wide coverage of the *P–z* plane is essential to any modelling of the radio luminosity function (Rawlings 2002). The combination of CoNFIG, 3CRR, CENSORS and the Lynx and Hercules samples covers a large range of luminosity and redshift (Figs 8 and 9), providing a powerful basis from which to study FR I and FR II sources.

6.2 Source counts

The morphologically dependent source counts (Fig. 10) were compiled as described by Gendre & Wall (2008), from the CoNFIG and complementary samples.

As seen in Fig. 7, uncertain sources (which are extended but uncertain to whether they are FR I or FR II) have a luminosity distribution closer to that of FR II sources than FR I sources. Thus, we make the assumption to include uncertain sources into the FR II morphology group for the source count. This inclusion does not make any significant change from the source count of FR II sources only.

The FR II sources dominate the total count, except at low flux densities ($\log S_{1.4\,GHz} \lesssim -1.6$), where the FR I sources suddenly take over, constituting a significant portion of the mJy and sub-mJy
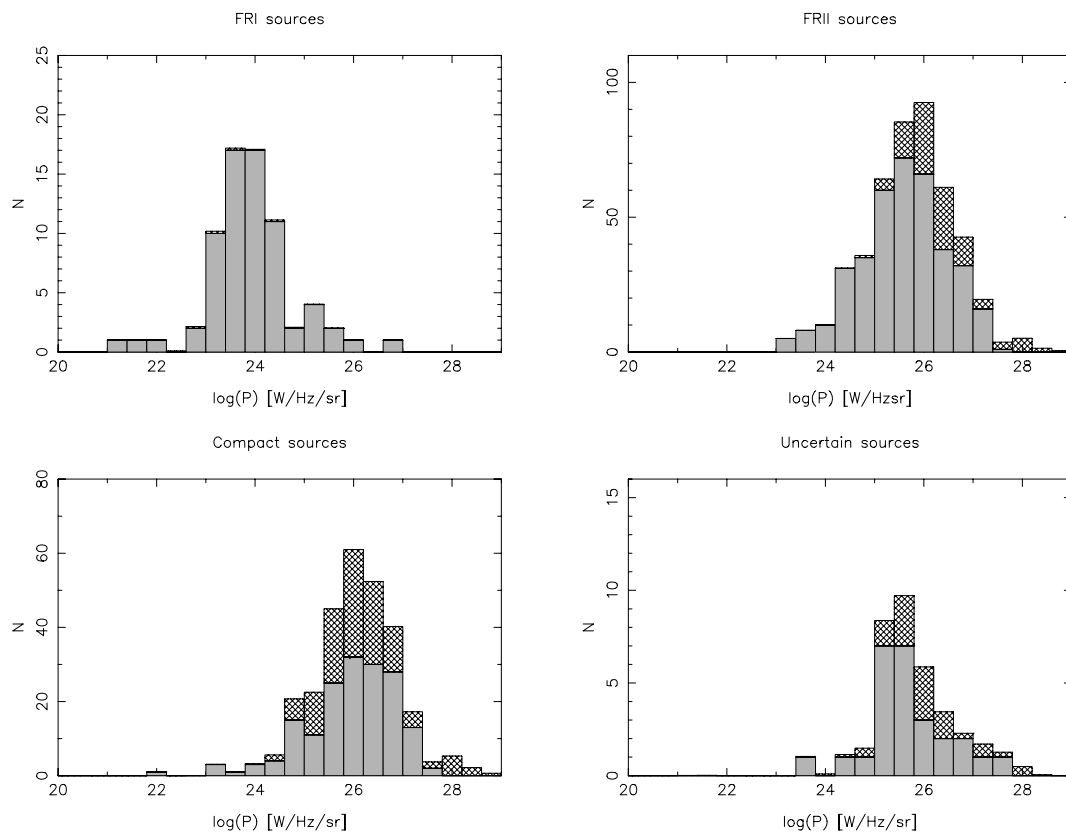
Figure 7. Luminosity distributions for compact and extended (FR I, FR II and uncertain) sources. The cross-hatched columns represent the estimated contribution to each luminosity bin of sources with no redshift information available, following the method presented in Section 4.2
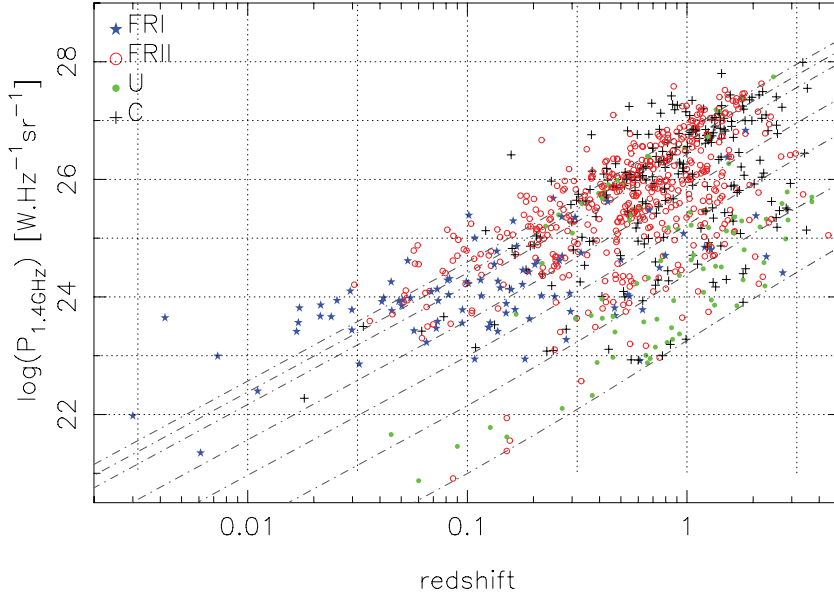
Figure 8. *P–z* plane coverage for the four CoNFIG samples, as well as the 3CRR, CENSORS and the Lynx and Hercules samples, by radio-morphological type (limited only to sources with estimated redshifts). The dot–dashed lines show the survey limits for each sample. Sources are identified by their radio morphological classification: FR Is, FR IIs, uncertain and compact sources are represented by blue stars, red circles, green dots and black crosses, respectively.
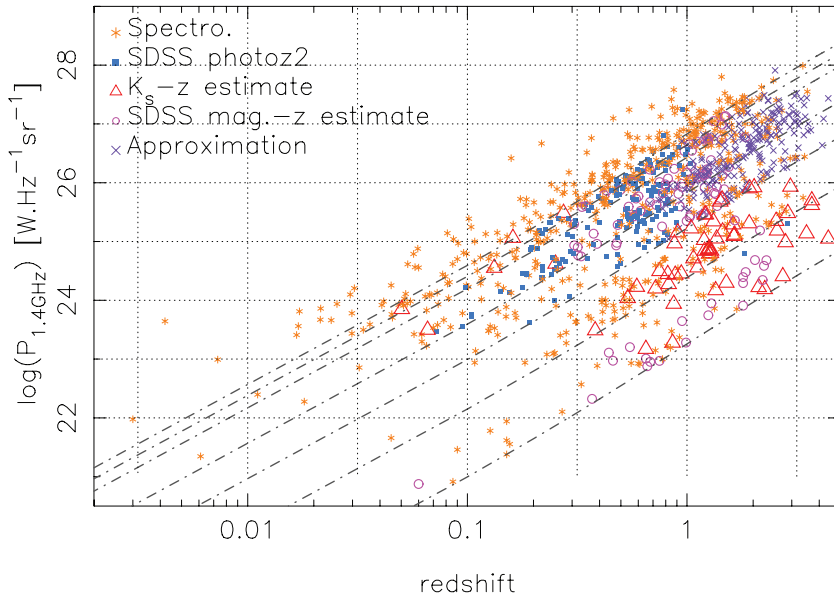
Figure 9. *P–z* plane coverage for the four CoNFIG samples, as well as the 3CRR, CENSORS and the Lynx and Hercules samples, by redshift type. The dot–dashed lines show the survey limits for each sample. Sources are identified by their redshift type: spectroscopic, SDSS *photoz2* photometric, K_S–z estimated and SDSS mag–z estimated redshift are represented by orange asterisks, blue squares, red triangles and pink circles, respectively. Sources with approximated redshifts, as described in Section 4.2, are represented by purple crosses.

sources in contrast to FR II sources. Since most of the FR I count at low flux densities is composed of low-luminosity sources at low redshift, our results show that FR I objects must undergo some mild evolution. This is consistent with the results of Sadler et al. (2007), who studied low power sources in the 2SLAQ survey (Richards et al. 2005) and found evidence that FR Is undergo significant evolution over $z < 0.7$. Our results also show that FR Is undergo less evolution than FR IIs, and they do not participate much in the source-count 'evolution bump' around $S_{1.4\,GHz} \sim 1$ Jy. This is in agreement with previous investigations stretching back to Longair (1966).

6.3 The local FR I/FR II RLFs

The RLFs were computed using the $1/V_{max}$ technique, in which, for each *P–z* bin, the space density of sources is given by:

$$\rho = \sum_{i=1}^{N} \frac{1}{V_i}, \qquad \sigma^2 = \sum_{i=1}^{N} \frac{1}{V_i^2}, \qquad (7)$$

where V_i is the largest volume in which the source could be observe in bin i.
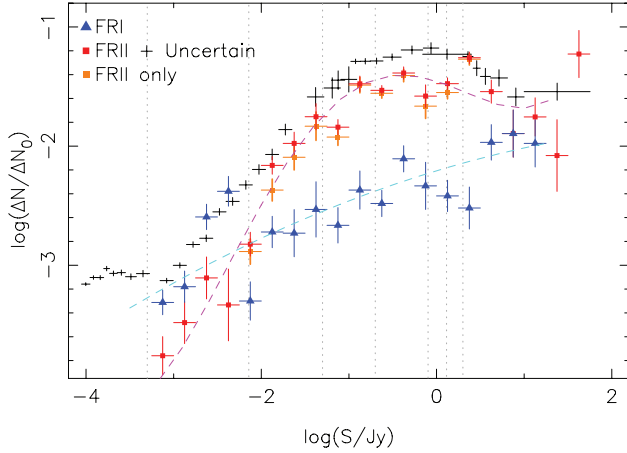
Figure 10. Relative differential source counts $\Delta N/\Delta N_0$ for FR I (blue triangles) and FR II+uncertain (red squares) sources. The count for FR II sources only is shown in orange squares, to illustrate the possible bias due to the inclusion of uncertain sources in the FR II group. Here, the normalization is given by $\Delta N_0 = 3618\Delta(S^{-1.5})$ (Jackson & Wall 1999) and the error bars correspond to $\sqrt{N}$, where N is the number of objects in each bin. The counts are fitted by a polynomial (dashed lines) to indicate the shapes of the counts. A 1.4-GHz source count, compiled from the data of Bridle et al. (1972), Machalski (1978), Hopkins et al. (2003) and Prandoni et al. (2001), is represented with crosses for comparison.
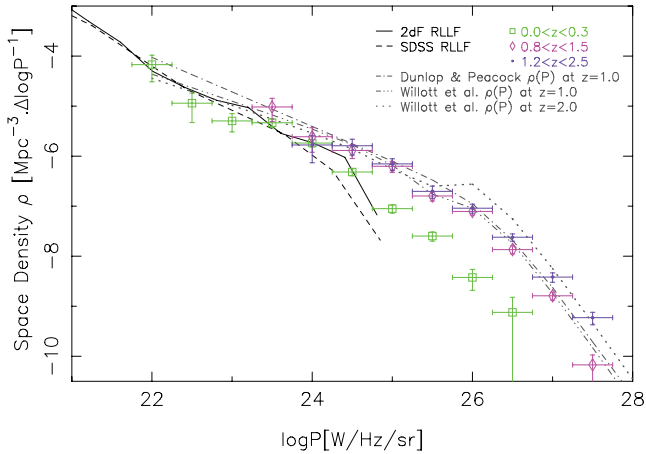
Figure 11. Luminosity function $\rho(P)$ computed from the four CoNFIG samples, as well as the 3CRR, CENSORS and the Lynx and Hercules samples. The radio LRLF for $z < 0.3$ for all extended sources is represented by open squares. The LRLF is consistent with both the LRLF of the 2dF survey (Sadler et al. 2002) and the SDSS (Best et al. 2005), shown by solid and dotted lines, respectively. In addition, the luminosity functions at $z = 1.0$ (in the interval $z = [0.8; 1.5]$) and at $z = 2.0$ (in the interval $z = [1.2; 2.5]$) are displayed by diamonds and dots, respectively. For comparison, the modelled RLFs from Dunlop & Peacock (1990) and Willott et al. (2001) at $z = 1.0$ are displayed in dot–dashed and triple-dot–dashed lines, respectively.

The general LRLF, defined here as the RLF for $z \leq 0.3$, is displayed in Fig. 11. It is consistent with both the LRLF of the 2dF survey (Sadler et al. 2002) and the SDSS (Best et al. 2005), and extends to significantly larger luminosities, because of the larger area covered by our bright samples.

In addition, the luminosity functions at $z = 1.0$ (in the interval $z = [0.8; 1.5]$) and at $z = 2.0$ (in the interval $z = [1.2; 2.5]$) were computed and compared with modelled RLFs from Dunlop &
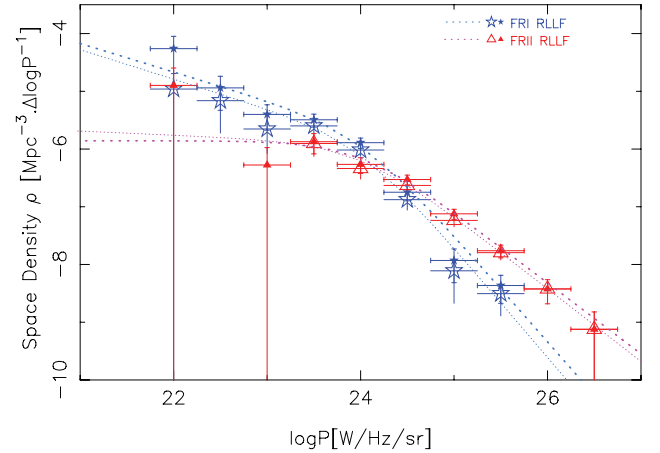
Figure 12. Local luminosity function $\rho(P)$ for FR Is and FR IIs, represented by stars and triangles, respectively. The values for both confirmed and possible FR I/FR II are shown by filled symbols and thick error bars, whereas the values for confirmed FR I/FR II only are displayed with open symbols and thin error bars. Data are fitted by a broken power law, described by equation (8).

Peacock (1990) and Willott et al. (2001) at $z = 1.0$. The CoNFIG RLF agrees well with both models.

The LRLFs for each population were computed and fitted, using the method of least-squares, by a broken power law, to provide parametric representations:

$$\rho(P) = \rho_0 \left[\left(\frac{P}{P^*} \right)^\alpha + \left(\frac{P}{P^*} \right)^\beta \right]^{-1}, \tag{8}$$

where $\log(P^*) = 24.0$ is the break luminosity, determined by visual inspection of the LRLFs. These LRLF models are plotted in Fig. 12.

The FR I and FR II LRLFs show apparent differences, such as the flattening of the FR II LRLF at lower powers and the steeper slope of the FR I LRLF at higher power. Overall, these LRLFs suggest that, locally, FR I and FR II sources constitute two distinct populations. However, these local space densities do not indicate any sharp luminosity divide between FR Is and FR IIs: at higher power ($\log P_{1.4\,\mathrm{GHz}} \gtrsim 25.0$) the FR II LRLF is only a factor of $\sim$3–4 higher than for FR Is and the two population show a large degree of overlap at intermediate powers.

Because most of the approximate redshifts (Section 4.2) are greater than $z = 0.3$, the results of the LRLF are completely unaffected by redshift uncertainties.

6.4 FR I/FR II evolution

The RLF for combined confirmed and possible sources for each population was then computed for different redshift bins ($z = [0.3; 0.8]$, $z = [0.8; 1.5]$ and $z = [1.2; 2.5]$). In order to account for data with no redshift information, the random redshift assignment technique described in Section 4.2 was used. This process was repeated 1000 times and the final RLF was computed by averaging the results.

For each population, the space density enhancement above the local value was computed. FR I sources (Fig. 13) show an enhancement of a factor of 7 to 10 in the interval $z = [0.8; 1.5]$ for high-luminosity sources ($\log P_{1.4\,\mathrm{GHz}} \geq 24.0\,\mathrm{W\,Hz^{-1}\,sr^{-1}}$), in agreement with the results of Rigby et al. (2008). This enhancement remains present at redshifts up to 2.5.
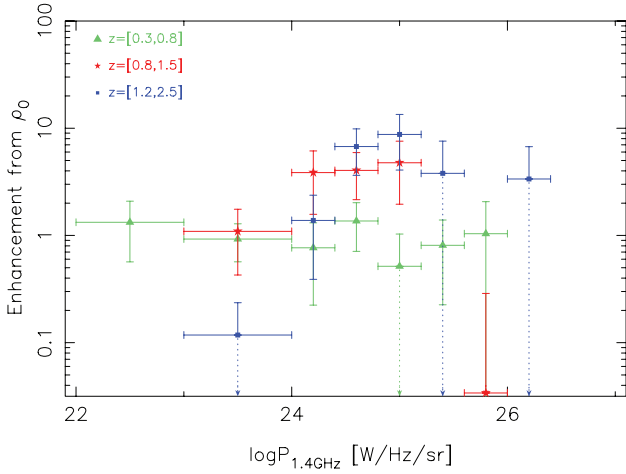
Figure 13. Space density enhancement for confirmed+possible FR I sources for different redshift bins: $z = [0.3:0.8]$ in triangles, $z = [0.8:1.5]$ in stars and $z = [1.2:2.5]$ in squares. An enhancement of a factor of 7 to 10 is seen at $z = 1.0$ for high-luminosity sources ($\log P_{1.4\,GHz} \geq 24.5$ W Hz^{-1} sr^{-1}), in agreement with Rigby et al. (2008). This enhancement appears to continue to higher redshifts.

A comparison of the space density enhancement for FR I and FR II sources in the same redshift bins is shown in Fig. 14. The overall behaviour of the enhancement with luminosity of FR I and FR II sources is very similar, with little or no enhancement in the interval $z = [0.3; 0.8]$ and up to a factor of 10 enhancement for higher luminosity sources in higher redshift bins. Both populations show similar enhancement history, hinting at a common mechanism governing the luminosity-dependent evolution. The RLFs were also computed for confirmed source only, and show the same overall trends.

In Fig. 15, we investigated the impact of the approximate redshift selection method. We compared RLFs in the ranges $z = [0.8; 1.5]$ and $z = [1.2; 2.5]$ from the CoNFIG FR II subsample, where the approximate redshifts were drawn using the distributions in which all sources with no redshift were either distributed homogeneously within the given range (to estimate the maximum space densities) or ignored (equivalent to setting all of them outside this range, hence giving minimum space densities).

In the range $z = [0.8; 1.5]$, the RLFs computed using approximate redshifts distributed homogeneously and ignored differ by a factor of 2.5, which is comparable to the size of the error estimates in the LRLF and RLF computed in this paper. The data and method therefore give a reasonably reliable estimate of the RLF in this redshift range, across all radio powers.
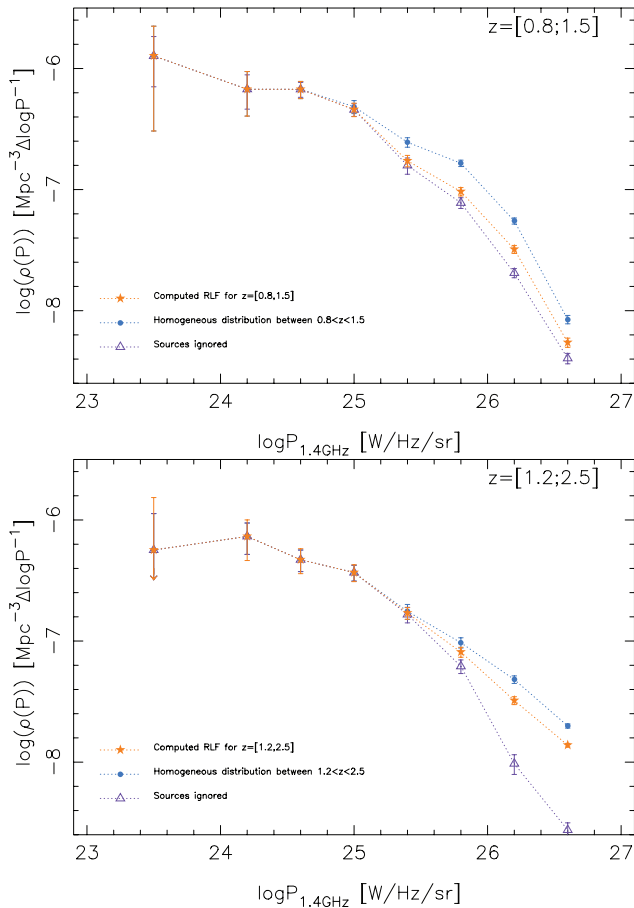
In the range $z = [1.2; 2.5]$ the approximate redshifts distribution method used in this paper gives results close to the maximal density calculated, whilst the minimal density lies significantly below this at high radio powers. This is because most of the approximated redshifts lie in this redshift range (as expected since the sources have $z_{lim} \simeq 1$) so the minimal density method provides a significant underestimate. The data allow an acceptable estimate of the RLF in this redshift range, but at higher powers ($\log P_{1.4\,GHz} \geq 26.0$) significant uncertainties remain.

7 SUMMARY

In this paper, we first described the latest steps in the construction of the CoNFIG catalogue, including new VLA observations. The
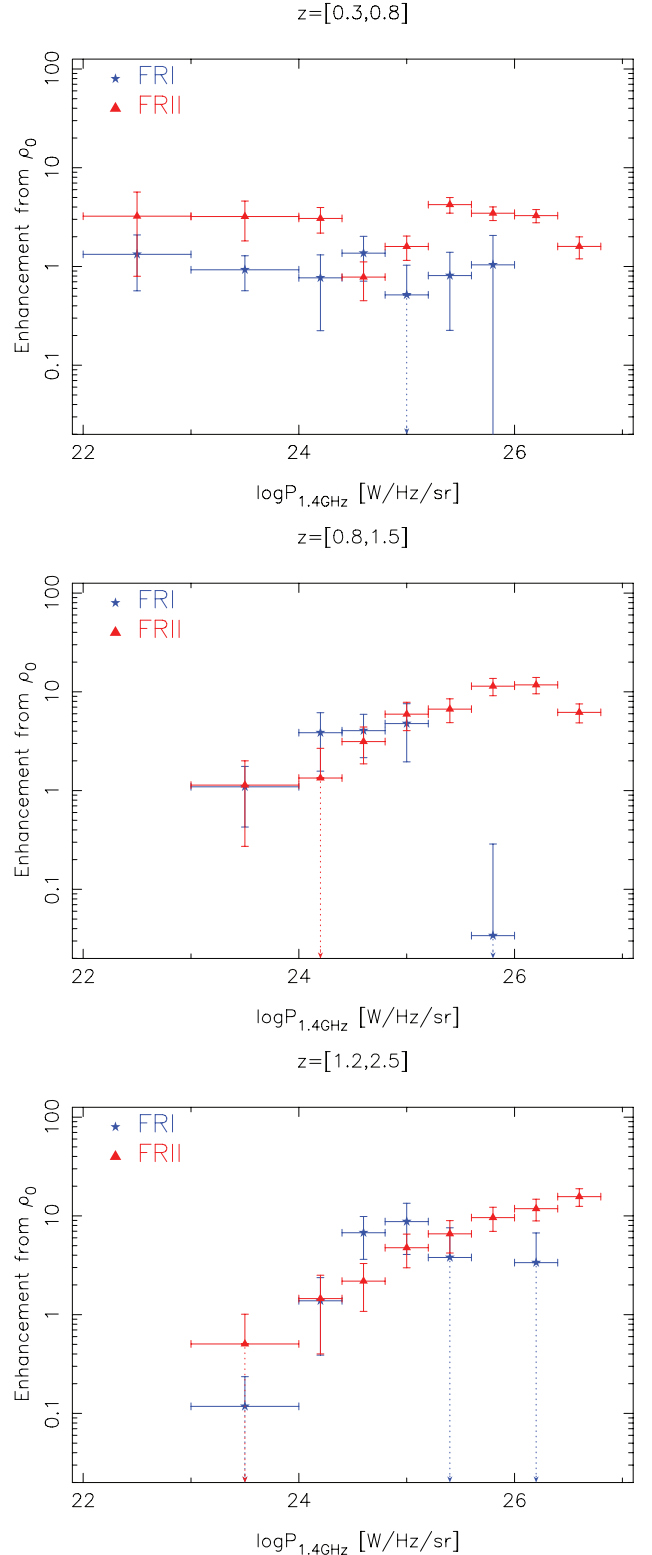
Figure 14. Comparison of the space density enhancement between confirmed+possible FR I (stars) and FR II (triangles) sources, for different redshift bins ($z = [0.3:0.8]$, $z = [0.8:1.5]$ and $z = [1.2:2.5]$). For FR Is with $\log P_{1.4\,GHz} \geq 26.0$ and FR IIs with $\log P_{1.4\,GHz} \leq 23.0$ and $\log P_{1.4\,GHz} \geq 27.0$, the value of the LRLF was extrapolated from the power-law fit described in Section 6.4. Both populations show similar enhancement history, hinting at a common mechanism governing the luminosity-dependent evolution.

Figure 15. FR II RLFs in the ranges $z = [0.8; 1.5]$ and $z = [1.2; 2.5]$ where the approximate redshifts were drawn using various distributions, in which all sources with no redshift were either approximated as described in Section 4.2 (stars), distributed homogeneously in the given range (dots) or ignored (triangles).

catalogue now consists of 859 sources in four samples (CoNFIG-1, -2, -3 and -4 with flux density limits $S_{1.4\,GHz} = 1.3, 0.8, 0.2$ and 0.05 Jy, respectively) and is 95.7 per cent complete for radio morphologies. 74.3 per cent of the sources have redshift information. Optical counterpart identifications were obtained from the SDSS and 2MASS catalogues for 74.6 and 26.8 per cent of the sources, respectively. Spectroscopic redshift information was retrieved from SDSS and the SIMBAD data base, while photometric redshifts (or redshift estimates) were compiled from the SDSS *photoz2* catalogue, or using a K_S–z or SDSS mag–z relation.

Combining CoNFIG with 3CRR, CENSORS and the Lynx and Hercules samples, the comparative distribution and evolution of FR I and FR II sources were investigated. The conclusions of this preliminary study are as follows.

(i) The FR II sources dominate the total count, except at low flux densities ($\log S_{1.4\,GHz} \lesssim -1.6$), where the FR I sources suddenly take over, constituting a significant portion of the mJy and sub-mJy sources in contrast to FR II sources.

(ii) The FR I and FR II LRLFs show apparent differences, suggesting that, locally, FR I and FR II sources constitute two distinct populations. However, they do not indicate any sharp luminosity divide between FR Is and FR IIs.

(iii) The FR I RLF shows an enhancement of a factor 7-10 over the local value, which continues to higher redshifts. This result is in agreement with the findings of Rigby et al. (2008).

(iv) The comparison of space density enhancement between FR I and FR II sources at various redshifts does not show any significant differences, suggesting a common mechanism governing the luminosity-dependent evolution.

REFERENCES

Abazajian K. N. et al., 2009, ApJS, 182, 543
Antonuccio-Delogu V., Silk J., 2008, MNRAS, 389, 1750
Baum S. A., Heckman T. M., 1989, ApJ, 336, 681
Beasley A. J., Gordon D., Peck A. B., Petrov L., MacMillan D. S., Fomalont E. B., Ma C., 2002, ApJS, 141, 13
Best P. N., Arts J. N., Röttgering H. J. A., Rengelink R., Brookes M. H., Wall J., 2003, MNRAS, 346, 627
Best P. N., Kauffmann G., Heckman T. M., Ivezić Z., 2005, MNRAS, 362, 9
Best P. N., Kaiser C. R., Heckman T. M., Kauffmann G., 2006, MNRAS, 368, 67
Bicknell G. V., 1995, ApJS, 101, 29
Bridle A. H., Davis M. M., Fomalont E. B., Lequeux J., 1972, AJ, 77, 1401
Brookes M. H., Best P. N., Rengelink R., Röttgering H. J. A., 2006, MNRAS, 366, 1265
Capetti A., Fanti R., Parma P., 1995, A&A, 300, 643
Condon J. J., Cotton W. D., Greisen E. W., Yin Q. F., Perley R. A., Taylor G. B., Broderick J. J., 1998, AJ, 115, 1693
Cowie L. L., Songaila A., Hu E. M., Cohen J. G., 1996, AJ, 112, 839
Dunlop J. S., Peacock J. A., 1990, MNRAS, 247, 19
Fanaroff B. L., Riley J. M., 1974, MNRAS, 167, 31P
Fomalont E., Petrov L., MacMillan D. S., Gordon D., Ma C., 2003, AJ, 126, 2562
Gendre M. A., Wall J. V., 2008, MNRAS, 390, 819
Granato G. L., Silva L., Monaco P., Panuzzo P., Salucci P., De Zotti G., Danese L., 2001, MNRAS, 324, 757
Hill G. J., Lilly S. J., 1991, ApJ, 367, 1
Hopkins A. M., Afonso J., Chan B., Cram L. E., Georgakakis A., Mobasher B., 2003, AJ, 125, 465
Jackson C. A., Wall J. V., 1999, MNRAS, 304, 160
Kimball A. E., Ivezić Z., 2008, AJ, 136, 684
Klamer I. J., Ekers R. D., Sadler E. M., Hunstead R. W., 2004, ApJ, 612, L97

Kovalev Y. Y., Petrov L., Fomalont E. B., Gordon D., 2007, AJ, 133, 1236

Laing R. A., Riley J. M., Longair M. S., 1983, MNRAS, 204, 151

Leahy J. P., 1993, in Rser H.-J., Meisenheimer K., eds, Jets in Extragalactic Radio Sources. Springer-Verlag, Heidelberg, p. 1

Longair M. S., 1966, MNRAS, 133, 421

Machalski J., 1978, A&A, 65, 157

Oyaizu H., Lima M., Cunha C. E., Lin H., Frieman J., Sheldon E. S., 2008, ApJ, 674, 7680

Parma P. et al., 1992, in Burgarella D., Livio M., O'Dea C., eds, Poster Papers from the Space Telescope Science Institute Symp., Astrophysical Jets. Space Telescope Science Institute, Baltimore, p. 30

Pearson T. J., Readhead A. C. S., 1988, ApJ, 328, 114

Petrov L., Kovalev Y. Y., Fomalont E. B., Gordon D., 2006, AJ, 131, 1872

Prandoni I., Gregorini L., Parma P., de Ruiter H. R., Vettolani G., Wieringa M. H., Ekers R. D., 2001, A&A, 365, 392

Quilis V., Bower R. G., Balogh M. L., 2001, MNRAS, 328, 1091

Rawlings S., 2002, in Pramesh Rao A., Swarup G., Gopal-Krishna, eds, Proc. IAU Symp. 199, The Universe at Low Radio Frequencies. Astron. Soc. Pac., San Francisco, p. 34

Rawlings S., Saunders R., Eales S. A., Mackay C. D., 1989, MNRAS, 240, 701

Richards G. T. et al., 2005, MNRAS, 360, 839

Rigby E. E., Snellen I. A. G., Best P. N., 2007, MNRAS, 380, 1449

Rigby E. E., Best P. N., Snellen I. A. G., 2008, MNRAS, 385, 310

Sadler E. M. et al., 2002, MNRAS, 329, 227

Sadler E. M. et al., 2007, MNRAS, 381, 211

Schawinski K. et al., 2009, AJ, 690, 1672

Silk J., Rees M. J., 1998, A&A, 331, 1

Skrutskie M. F. et al., 2006, AJ, 131, 1163

Snellen I. A. G., Best P. N., 2001, MNRAS, 328, 897

van Breugel W., Fragile C., Croft S., de Vries W., Anninos P., Murray S., 2004, in Storchi-Bergmann T., Ho L. C., Schmitt H. R., Proc. IAU Symp. 222, The Interplay among Black Holes Stars and ISM in Galactic Nuclei. Cambridge Univ. Press, Cambridge, p. 485

Wall J. V., Jackson C. A., 1997, MNRAS, 290, 17

White R. L., Becker R. H., Helfand D. J., Gregg M. D., 1997, ApJ, 475, 479

Willott C. J., Rawlings S., Blundell K. M., Lacy M., 2001, MNRAS, 322, 536

Willott C. J., Rawlings S., Jarvis M. J., Blundell K. M., 2003, MNRAS, 339, 173

York D. G. et al., 2000, AJ, 120, 1579

SUPPORTING INFORMATION

Additional Supporting Information may be found in the online version of this article:

Appendix A. The CoNFIG catalogue.
Appendix B. Contour plots.

Please note: Wiley-Blackwell are not responsible for the content or functionality of any supporting materials supplied by the authors. Any queries (other than missing material) should be directed to the corresponding author for the article.

This paper has been typeset from a TeX/LaTeX file prepared by the author.